Smart Mater. Struct. 5 (1996) 723–730. Printed in the UK

Active aeroelastic tailoring of an adaptive Flexspar stabilator

R Barrett

Auburn University, Auburn, Alabama 36849, USA

Received 9 January 1996, accepted for publication 1 August 1996

Abstract. The aeroservoelastic properties of a new class of adaptive aeronautical surfaces are detailed. These new active surfaces use the newly invented Flexspar configuration which employs a high-strength main spar around which an aerodynamic shell is pivoted. Within the aerodynamic shell, a piezoelectric actuator is mounted with one end bonded rigidly to the spar and the other attached to a point on the shell. As the piezoelectric element is energized, the pitch angle of the shell is changed. Adjacent to the piezoelectric element, a sensor is used to determine the position of the shell. A simple feedback loop connecting the sensor and actuator provides a high degree of stability. Inertial and aerodynamic coupling are minimized by collocating the pitch axis, aerodynamic center and center of gravity. Laminated plate theory estimations are used with basic kinematic expressions for relating piezoelectric flexure to shell pitch angle change. Wind tunnel test results demonstrate that stable deflections up to $\pm 11^{\circ}$ are possible. By using an adaptive positioning system, the aerodynamic shell may be moved with respect to the main spar. This modification lends aeroservoelastic characteristics to the system. Accordingly, as the quarter-chord of the shell is moved forward of the pitch axis, small pitch deflections are effectively magnified with increasing air speed. Experimental testing of an aeroservoelastically coupled wing specimen showed magnification of pitch deflections from $\pm 11^{\circ}$ to $\pm 16^{\circ}$ and good correlation with theory.

Nomenclature

A, B, D	extensional, coupling and bending stiffness matrices
c	mean geometric chord
C_L	lift coefficient
$C_{L\alpha}$	lift curve slope
e	pitch axis—quarter chord eccentricity
E_3	through thickness electric field
E_L, E_T	longitudinal and transverse element stiffness
K	rotational stiffness
l	length of Flexspar component
q	dynamic pressure
R	control effectiveness ratio
S	stabilator surface area
t	thickness
V	air speed
α_o	base angle of attack
α_e	aeroservoelastic angle of attack
κ_{ij}	ijth laminate curvature
Λ_i	ith direction actuator free strains
ϕ_a	active pitch angle (with no aeroservoelastic magnification)

Subscripts

a	actuator
b	bond
o	original or base conditions
s	substrate
tot	total

1. Introduction

Flight control has been one of the major concerns of aviation enthusiasts since the invention of the first aircraft. The dawn of controlled flight saw early aviators shifting weight and pulling wires to steer their crafts. In these early days, various types of twisting, all-moving and flapped wing sections were used to manipulate air loads. As time progressed, the control surfaces became more sophisticated and today aircraft designers have an impressive array of actuators, materials and surface designs which may be used. One of the newer types of control surface actuators uses adaptive materials. In many ways, adaptive flight control surfaces are novel, modern devices which are unique and new; however, such structures have been in flight for more than 270 million years in the animal world. Because the adaptive actuators and the aircraft structure are intimately integrated, flight control by using camber and twist changes (as with bird wings) are possible. In 1989, the first of these adaptive aerodynamic studies was conducted on a series of bending-twist and extension-twist coupled aerodynamic plates. Crawley *et al* [1] successfully showed that piezoelectric elements

0964-1726/96/060723+08$19.50

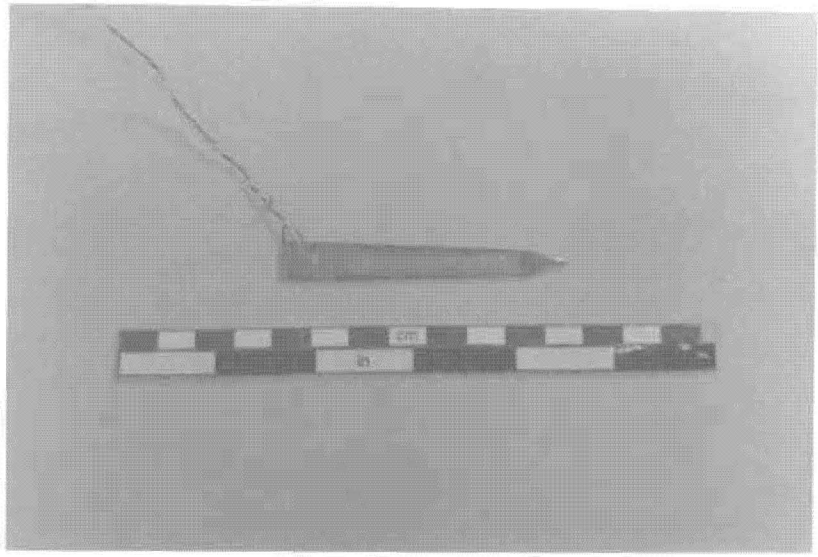

Figure 1. Typical Flexspar main spar and active element (from TOW missile of [23]).

could actively bend or actively extend these coupled plates. As a result, twist motions would be generated which would, in turn, alter the loading across the span of the plate. Following this early work, a number of experimenters showed that piezoelectric actuators could be integrated into aerodynamic surfaces to induce twist and camber changes. Many of these studies were centered on vibration amelioration and flutter suppression. However, many technologists continued to explore different types of aeroelastic control [2–5]. Various control schemes were devised for using skin-bonded elements to change the camber and twist of wings. The effects of wing sweep on active aeroservoelastic performance were included by Ehlers and Weisshaar [6]. At about the same time, a new manufacturing method for piezoelectric elements was discovered which would lend highly orthotropic characteristics to otherwise isotropic piezoelectric sheets. These directionally attached piezoelectric (DAP) elements were shown to have orthotropy ratios in excess of 50 [7]. Accordingly, several experiments were conducted to show that inherent structural or geometric coupling (as was the case with the bending-twist or extension-twist aerodynamic surfaces) was no longer necessary to induce active twist deflections in flight control surfaces. Instead, the DAP elements could be arranged so as to generate directly a torsional shear flow which would result in a twist deflection. The first of these studies was conducted on helicopter rotor blades [7–9]. Although only small static twist deflections were generated ($\pm 0.1^\circ$ at 600 V mm^{-1}), the principles of active blade twist manipulation were proven. Six years of follow-on work have since been conducted in the area of active helicopter rotor blade twist manipulation [10–12]. The culmination of this tireless endeavor has been an improvement in static twist deflection to nearly $\pm 0.2^\circ$ at 600 V mm^{-1} [13]. Because these twist levels are so low, many investigators have looked into high-authority actuators for a greater degree of control. One of the most common high-authority devices has been the active servoflap. Conceived in 1989 by Spangler and Hall, the active servoflap has demonstrated high lift coefficient changes in a small package [14]. This device performs admirably in attached flow as is found in helicopters; however, at high angles of attack, like those experienced by missiles, the surface locks in a hard-over deflection. Accordingly, flight control devices for missiles and other vehicles which use low aspect ratio surfaces need another type of adaptive surface design for flight control.

In early 1991, a new type of missile flight control surface was invented [9]. This device employed a twist-active DAP torque plate which was bonded to a structurally stiff main spar. Tests showed that relatively large static pitch deflections ($\pm 4.5^\circ$) could be generated [15, 16]. Although deflections of this order of magnitude are fine for many types of flight control, still higher deflection levels are needed for many applications. Accordingly, an initial study into aeroelastic tailoring of torque plate fins was made in 1992 [17, 18]. This early study demonstrated that air loads could successfully be used to magnify pitch deflections. Unfortunately, along with pitch angle magnification came divergence. As a result, all of the subsequent torque plate research has been on control surfaces which are not aeroelastically coupled. Still, significant advances have been made without coupling.

Among these advances have been the invention of the free-spar torque plate fin [19, 20] and the Flexspar fin [21]. The free-spar design has shown the highest pitch deflection levels of any torque plate configuration, up to $\pm 8^\circ$ with a break frequency in excess of 50 Hz. This prototype 5" span by 2" chord graphite–epoxy fin exhibited stable deflections with air speed and no flutter, buffet or divergence tendencies [19–21]. Because still greater pitch deflections are necessary for many types of missiles, a new type of actuator configuration dubbed the Flexspar was invented. Accordingly, this paper will lay out the fundamentals of the Flexspar configuration and present data on a new type of active aeroservoelastic tailoring method.

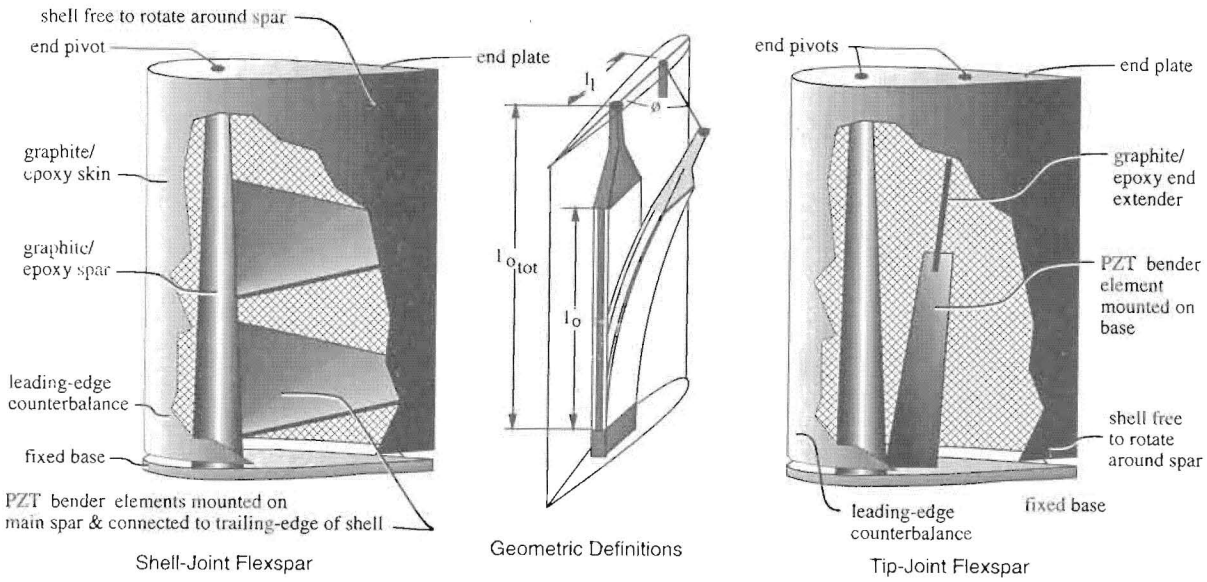

Figure 2. Shell-joint and tip-joint Flexspar configurations.

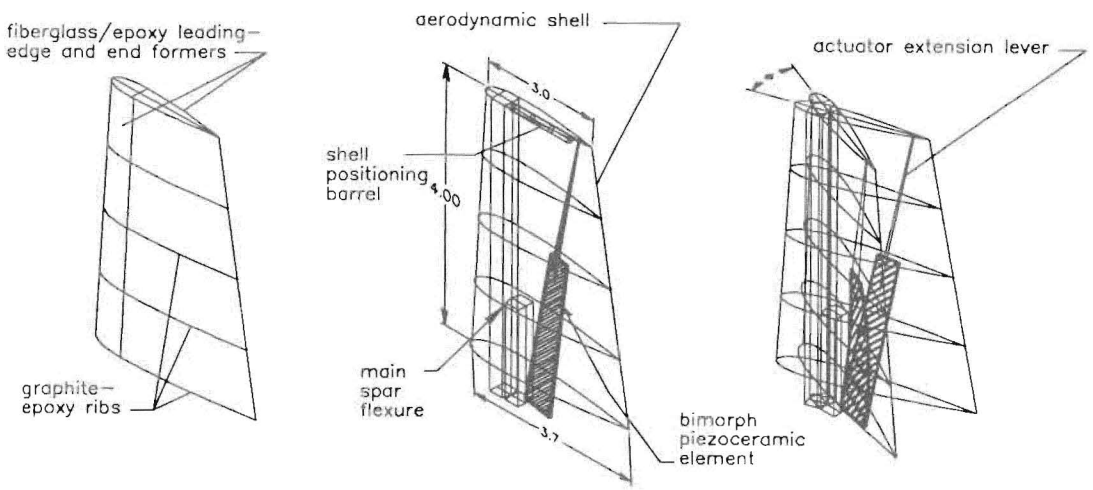

Figure 3. Adaptive shell-positioning Flexspar arrangement.

2. Tip-joint Flexspar design and modelling

The Flexspar design is based on a single bimorph actuator which drives an aerodynamic shell in pitch. Within the aerodynamic shell, a structurally stiff main spar provides support for a pair of pivots which form a rotational axis. For subsonic applications, the main spar, center of gravity and aerodynamic center are usually collocated along the quarter-chord of the aerodynamic shell. The base of the bimorph bender is rigidly fixed to the main spar, while the tip is joined to the shell. Figure 1 shows a typical main spar and bimorph actuator prior to structural integration.

There are two main configurations of Flexspar fins. The first, the shell-joint Flexspar has a bimorph bender element which is rigidly bonded to the main spar and connects to the shell in a chordiwise direction. This configuration is generally used for high-stiffness low-deflection applications. The second configuration is the tip-joint Flexspar. This uses a bimorph bender element which is mounted at the root of the fixed base and connects to the tip of the movable shell. Much larger deflections are attainable from the tip-joint configuration. Figure 2 shows a typical tip-joint configuration with geometric nomenclature for analysis.

2.1. Tip-joint Flexspar

Laminated plate theory has been used to analyse adaptive plate structures successfully for several decades. Using the conventional laminated plate theory assumptions laid out by Jones [25] the element curvature may be estimated. If one examines the balance of externally applied moments and forces (ex), those applied by the actuator (a) and thermally induced forces and moments (t), then the static behavior of

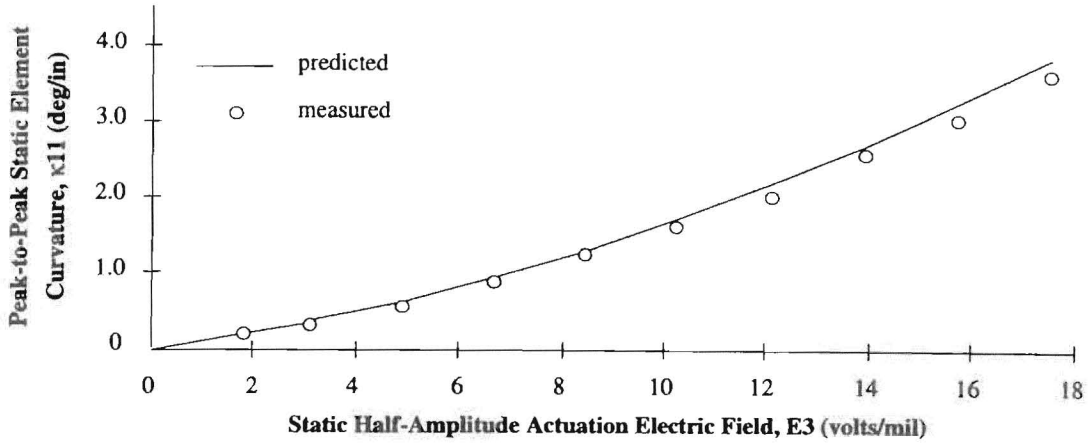

Figure 4. Actuator beam flexural test results.

the laminate may be described as follows:

$$\begin{Bmatrix} N \\ M \end{Bmatrix}_{ex} + \begin{Bmatrix} N \\ M \end{Bmatrix}_{a} + \begin{Bmatrix} N \\ M \end{Bmatrix}_{t} = \begin{bmatrix} \mathbf{A} & \mathbf{B} \\ \mathbf{B} & \mathbf{D} \end{bmatrix}_{l} \begin{Bmatrix} \epsilon \\ \kappa \end{Bmatrix}_{l} \tag{1}$$

where

$$N = \int \sigma \, dz \qquad M = \int \sigma z \, dz.$$

For an unloaded, simple bender configuration composed of symmetric isotropic conventionally attached actuator sheets, equation (1) can be decomposed into its components. Considering an elevated temperature cure, the axial compressive stresses in the actuator sheets and the tensile stresses in the substrate may be considerable. Equation (2) shows the relationship between this bending curvature, κ, axial strain, ϵ, thermally induced axial strains and the active bending induced by antisymmetric actuation of the piezoceramic sheets.

$$\begin{aligned} &\begin{bmatrix} A_{11}+A_{12} & 0 \\ 0 & D_{11}+D_{12} \end{bmatrix}_{lam} \begin{Bmatrix} \epsilon \\ \kappa \end{Bmatrix} \\ &\quad = \begin{bmatrix} A_{11}+A_{12} & 0 \\ 0 & D_{11}+D_{12} \end{bmatrix}_{a} \begin{Bmatrix} \alpha\Delta T \\ 0 \end{Bmatrix}_{a} \\ &\begin{bmatrix} A_{11}+A_{12} & 0 \\ 0 & D_{11}+D_{12} \end{bmatrix}_{s} \begin{Bmatrix} \alpha\Delta T \\ 0 \end{Bmatrix}_{s} \\ &\quad + \begin{bmatrix} 0 & B_{11}+B_{12} \\ B_{11}+B_{12} & 0 \end{bmatrix}_{a} \begin{Bmatrix} \Lambda \\ 0 \end{Bmatrix}. \end{aligned} \tag{2}$$

Assuming that a finite bond line with low stiffness connects a pair of piezoceramic sheets to an isotropic substrate, then the longitudinal curvature of the actuator element, κ_{11}, is as follows:

$$\kappa_{11} = E_a\left(t_s t_a + 2t_b t_a + t_a^2\right)\Lambda \Big/ \left[\frac{E_s t_s^3}{12} + E_a\left(\frac{(t_s+2t_b)^2 t_a}{2} + (t_s+2t_b)t_a^2 + \frac{2}{3}t_a^3\right)\right]. \tag{3}$$

If one considers the elevated temperature cure without premature resin cure, then the laminate strain can be estimated as follows:

$$\epsilon = \frac{2E_a t_a \alpha_a \Delta T + E_s t_s \alpha_s \Delta T}{2E_a t_a + E_s t_s}. \tag{4}$$

If the geometry of figure 2 is used in conjunction with the estimation for laminate curvature of equation (3), then the total rotational deflection, ϕ, may be obtained. Considering the geometry of figure 2, an estimate of how far the tip of the bender element moves without considering vertical motion due to curvature is given by:

$$d = \left(l_{o_{tot}} - \frac{\sin(\kappa l_0)}{\kappa}\right)\sin(\kappa l_o). \tag{5}$$

By including vertical height reduction and considering an ideal slip joint at the tip connector, the pitch angle, ϕ, may be estimated as a function of bimorph curvature, κ, and geometry.

$$\phi = 2\sin^{-1}\left[\left\{\frac{1-\cos(\kappa l_o)}{\kappa} + \left(l_{o_{tot}} - \frac{\sin(\kappa l_0)}{\kappa}\right) \times \sin(\kappa l_0)\right\} \Big/ 2l_1\right]. \tag{6}$$

2.2. Shell-joint Flexspar

If the bimorph element is tilted 90° (horizontal) from that shown in figure 2, and bonded to the shell of the stabilator, then a comparatively stiff, low-deflection actuator may be built. Borrowing the dimensional notation from figure 2, and using the bimorph curvature estimation of equation (3), the shell-joint pitch angle may be obtained from

$$\phi = \tan^{-1}\left[\left\{\frac{1-\cos(\kappa l_o)}{\kappa} + \left(l_{o_{tot}} - \frac{\sin(\kappa l_o)}{\kappa}\right) \times \sin(\kappa l_o)\right\} \Big/ l_{o_{tot}}\right]. \tag{7}$$

Examination of equation (7) shows that the deflections will be considerably smaller than those obtained for the tip-joint Flexspar configuration.

3. Control surface design and construction

As with earlier torque plate and Flexspar investigations, PZT-5H piezoceramic sheets were used to power the aerodynamic surface. Figure 3 shows the overall geometry

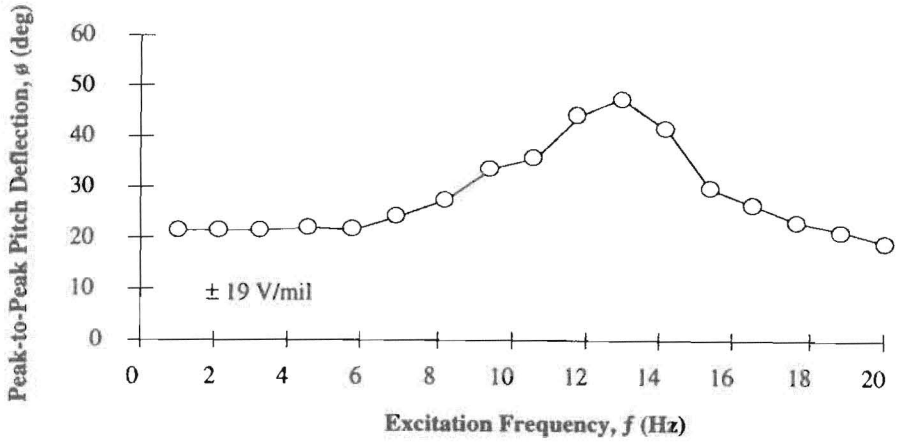

Figure 5. Flexspar fin pitch angle as a function of actuation frequency.

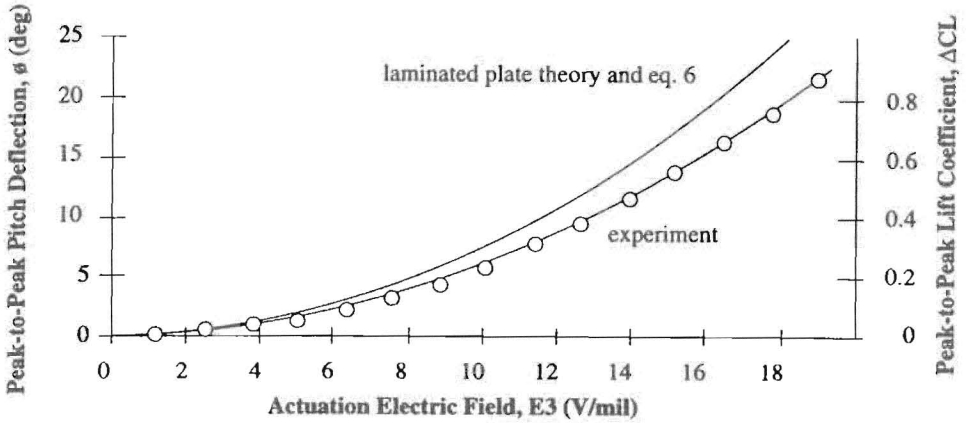

Figure 6. Active aerodynamic characteristics of the uncoupled Flexspar fin.

of the stabilator with the internal layout of the components. The piezoelectric bender was constructed from a pair of 7.5 mm PZT sheets bonded to a 2 mm brass substrate with Scotchweld™ adhesive tape in a 350°F cure under approximately 8 psi of pressure. The actuator element is 2.5" long with the root of the actuator element measuring 0.4" and the tip 0.3" wide. Masterbond™ conducting epoxy was used to make electrical contact with the nickel electroded faces of the PZT sheets. After the cure, the element was removed from curing jigs, deflashed and trimmed to tolerance. A protective root section made of style #120 fiberglass was added to provide protection for the leads and the base of the element. A graphite–epoxy extender measuring 1.8" was bonded to the tip of the actuator bimorph and the end of the shell. The main spar was constructed with a flexible Nylon hinge sandwiched between the structural material. The tip of the shell had a positioning barrel which could move the aerodynamic shell up to 20%c. The fully contracted position of the barrel collocated the fin aerodynamic center and the pitch axis. As the barrel was extended, the shell moved forward with respect to the pitch axis. This gave adaptive aeroservoelastic characteristics to the system. The shell positioning barrel was constructed from a 10 mm diameter Tinel™ alloy K shape memory alloy coil which was balanced by a conventional spring–steel coil. The position of the barrel was determined by a helical position sensor which was connected to a closed-loop controller.

The aerodynamic shell of figure 3 was constructed with a fiberglass leading-edge shell up to 30%c and tip shell from 85% to 100% of the span. Aft of the leading-edge shell a series of graphite ribs made from 1k tows was connected to the trailing-edge stiffener. The internal shell structure was covered with Micafilm aerodynamic skinning material.

4. Control surface testing and aeroelastic tailoring

The driving element of the Flexspar fin was tested for tip-bending deflection. A laser mirror was mounted on the end of the member and the deflections were measured. Figure 4 shows the test results as compared to the laminated plate theory estimations.

After the flexural characteristics of the actuator were verified, basic bench and wind tunnel tests were conducted on the entire fin. The mass moment of inertia of the

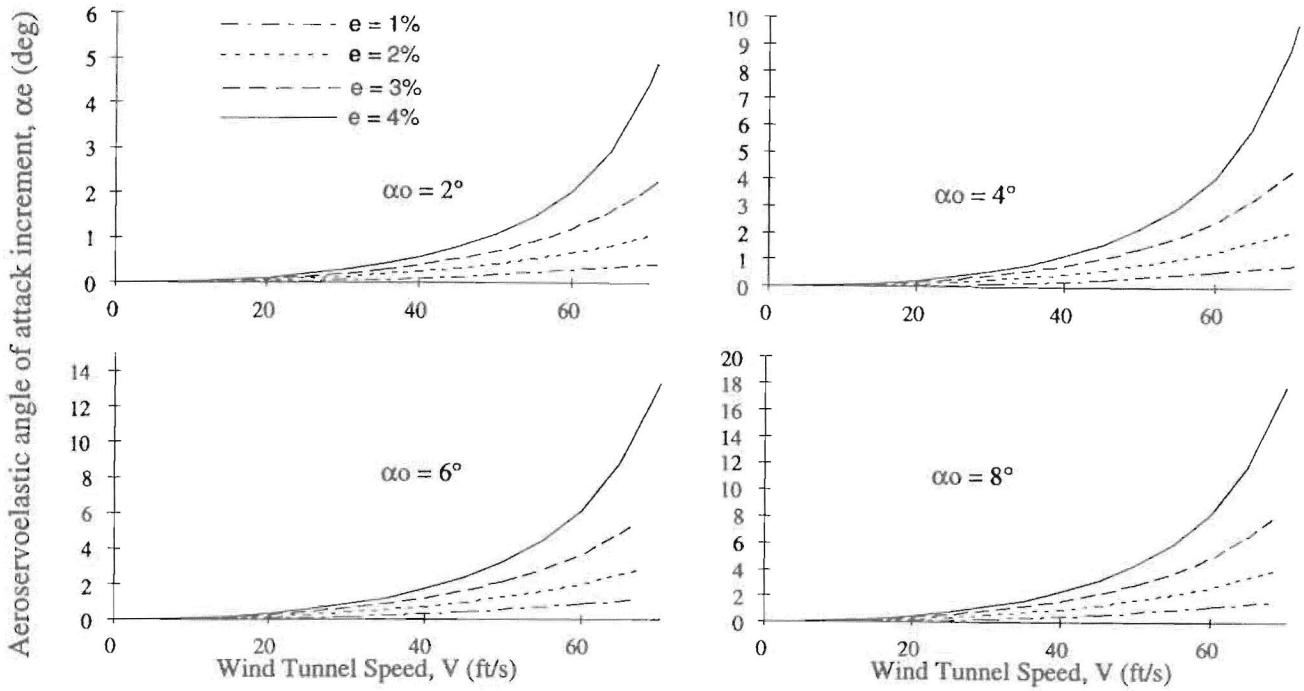

Figure 7. Aeroservoelastic angle of attack increment as a function of geometry, base conditions and aerodynamic forces.

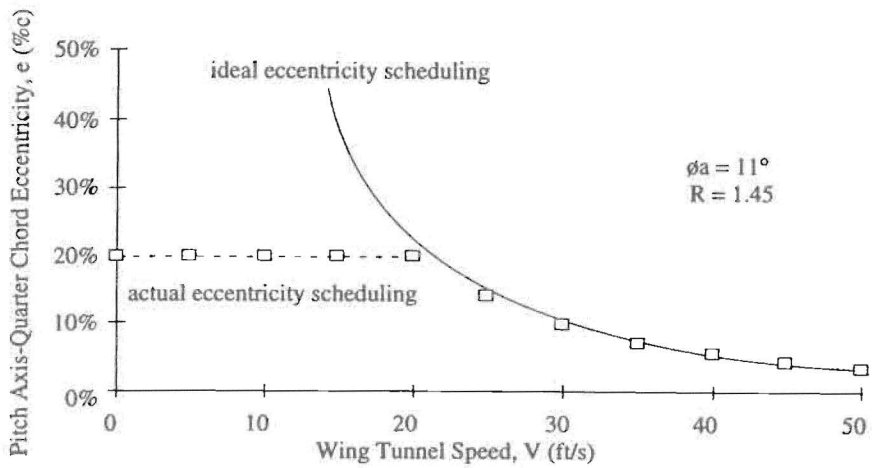

Figure 8. Eccentricity scheduling for a maximum aeroelastic angle of attack range of ±16°.

fin structure was determined to be 0.0132 lbm in^2 by performing a series of tests in a rotational spring rig. Dynamic testing showed that the low-deflection, passive rotational stiffness is approximately 0.0040 in lb deg^{-1}. Figure 5 shows the results of the dynamic bench testing.

Bench testing demonstrated a natural frequency of approximately 13 Hz. During testing, the shell pitch deflections grew so high that the fin was restrained by structural stops as it approached the natural frequency. This resulted in 'blunting' of the resonance peak of figure 5.

A series of aerodynamic tests were conducted on the Flexspar fin in the 1 ft × 1 ft model scale wind tunnel at Auburn University. Static deflection of the fin was measured by a position measurement bar mounted within the structure and by correlating the electrical measurements with laser rotation data. An estimate of the static deflection was made using equations (1) and (2) with no aeroelastic coupling (pitch axis and aerodynamic center were collocated). The testing was conducted in a pseudostatic condition with a 0.5 Hz sine signal driving the shell in pitch. Figure 6 shows the analytical estimations of pitch deflection and the experimental aerodynamic data.

From figure 6, it can be seen that the linear lift curve slope is approximately 0.041/deg. Because the aerodynamic profile is symmetric (modified NACA 0012), there is no zero-lift pitching moment about the quarter-chord. Further, the bench and wind tunnel test data are sufficient for prediction of the aeroservoelastic characteristics. Through a simple moment balance, the aeroservoelastic angle of attack increment α_e may be

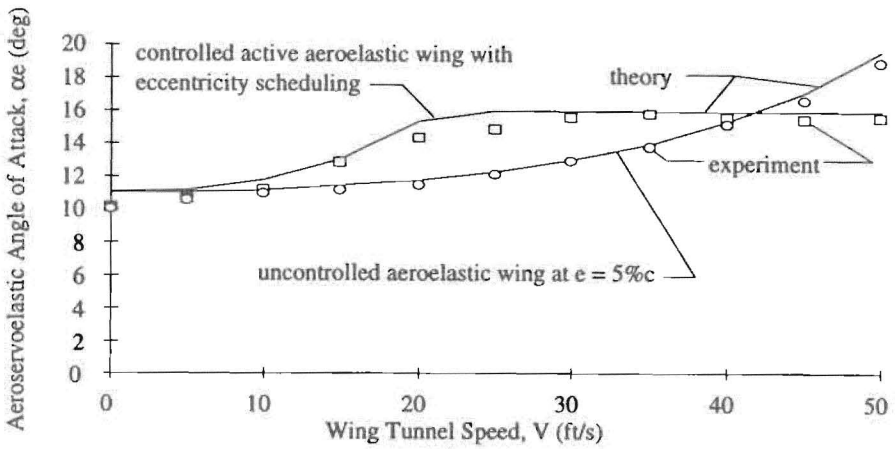

Figure 9. Comparison of steady aeroservoelastic angle of attack for a 5% offset and a scheduled offset as per figure 8.

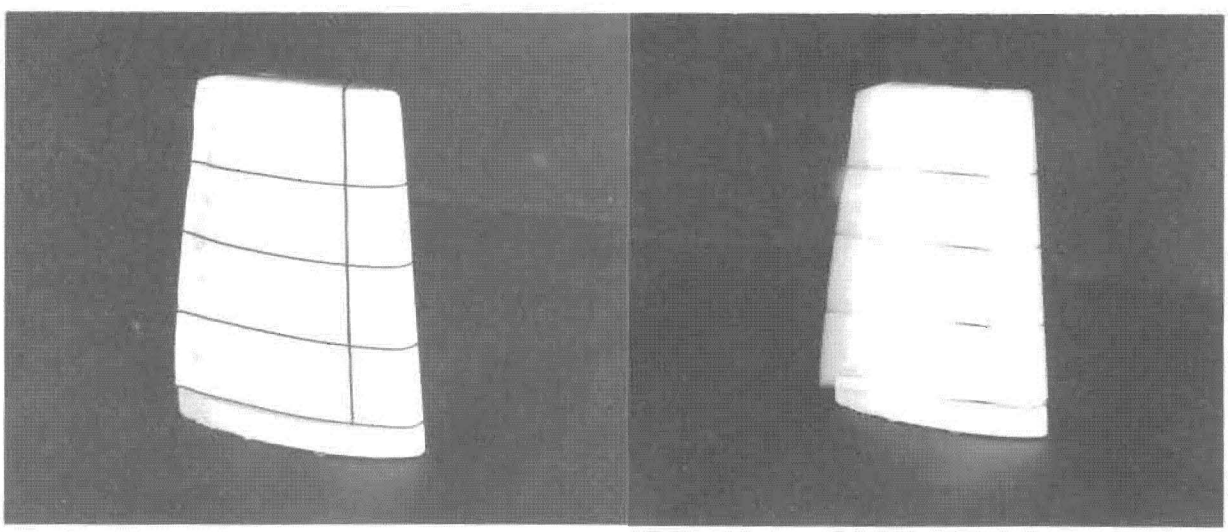

Figure 10. Static and dynamic Flexspar fin during wind tunnel testing.

determined.

$$\alpha_e = \frac{K_{tot}\phi_a - \bar{q}S\bar{c}eC_{L_\alpha}\alpha_o}{\bar{q}S\bar{c}eC_{L_\alpha} - K_{tot}}. \tag{8}$$

Equation (8) shows that the pitch axis quarter-chord eccentricity e, active pitch angle ϕ_a, dynamic pressure q, and base angle of attack α_o have a profound effect on the aeroservoelastic angle of attack increment, α_e. Using equation (8) it can be seen that large eccentricity can induce rapid divergence as shown in figure 7.

From figure 7, it can be seen that stable aeroservoelastic deflections cannot be attained by using a conventional approach to fin design. Accordingly, a specialized adjusting barrel was used to position the aerodynamic shell with respect to the pitch axis which is aligned with the main spar. This shell manipulation barrel may be contracted or extended so as to manipulate the fin eccentricity. Because aerodynamic control comes from the active pitch deflection ϕ_a, it is desirable to magnify this value to increase the control power of the system. The control effectiveness ratio R can be defined as: $R = \alpha_e/\phi_a$. Because the eccentricity may now be scheduled to hold a constant aeroservoelastic angle of attack increment, equation (4) may be rearranged to find e.

$$e = \frac{K_{tot}(R+1)}{\bar{q}S\bar{c}C_{L_\alpha}(R + \alpha_o/\phi_a)}. \tag{9}$$

From equation (9), it can be easily seen that at low air speed, the eccentricity tends to infinity (ideally). Because there are physical limitations in the system, the actual eccentricity of a given system will be truncated at a fixed level until the dynamic pressure increases.

A series of experiments was run with the shell positioning system activated. Because the uncoupled active deflections range up to $\pm 11°$ and the onset of stall starts at around $\pm 16°$ deflection, the control effectiveness ratio may be fixed at $R = 1.45$. Figure 8 shows actual and ideal eccentricity scheduling as a function of wind tunnel speed.

With the proper eccentricity scheduling in hand, the wing was tested to demonstrate the amount of stable aeroservoelastic magnification that may be obtained through the active positioning system. Figure 9 shows the aeroservoelastic angle of attack of the fin with a fixed 5% eccentricity and an appropriately scheduled offset.

Throughout the wind tunnel testing, the fin exhibited no flutter tendency as it was mass balanced about the quarter-chord of the aerodynamic shell. Also, the fin experienced no buffet as the flow over the fin was extremely smooth. The tunnel turbulence factor was determined to be less than 0.04. Figure 10 shows the static and dynamic Flexspar fin during wind tunnel testing.

5. Conclusions

This study has shown that laminated plate theory and kinematics can successfully predict the deflections generated by Flexspar flight control surface actuators with aeroservoelastic tailoring. Experimental model testing showed that pitch deflections up to $\pm 11°$ may be achieved with Flexspar control surfaces measuring 4" in span with a 3.33" mean geometric chord. Using a shell offset of up to 20%, the deflection magnitudes may be increased to and held at $\pm 16°$ at speeds greater than 25 ft s^{-1}.

Acknowledgments

The author would like to acknowledge the Auburn University School of Engineering and Aerospace Engineering Department for supporting this research, along with Dr Brian Chin and the Auburn University Materials Engineering Program. The author would also like to thank Fred Brozoski, Clifton Minter, Steven Williams and Steven Rose for helping with the construction and testing of Flexspar fins.

References

[1] Crawley E F, Lazarus K B and Warkentin D J 1989 Embedded actuation and processing in intelligent materials *2nd Int. Workshop on Composite Materials and Structures (Troy, NY) 1989*

[2] Lazarus K B, Crawley E F and Bohlmann J D 1990 Static aeroelastic control using strain actuated adaptive structures *Proc. First Joint US/Japan Conf. on Adaptive Structures (Maui, Hawaii) October 1990*

[3] Song O, Librescu L and Rogers C A 1991 Static aeroelasticity behavior of adaptive aircraft wing structures modeled as composite thin-walled beams *Int. Forum on Aeroelasticity and Structural Dynamics (Aachen, Germany) June 1991*

[4] Ehlers S M 1991 Aeroelastic behavior of an adaptive lifting surface *PhD Thesis* Purdue University

[5] Lazarus K B, Crawley E F and Lin C Y 1991 Fundamental mechanisms of aeroelastic control with control surface and strain actuation *Proc. 32nd AIAA/ASME/ASCE/AHS/ASC Structures, Structural Dynamics and Materials Conf. (Baltimore, MD) 1991* AIAA-91-0985-CP, pp 1817–31

[6] Ehlers S M and Weisshaar T A 1990 Static aeroelastic behavior of an adaptive laminated piezoelectric composite wing *AIAA J.* **28** 1611–23

[7] Barrett R M 1990 Intelligent rotor blade and structures development using directionally attached piezoelectric crystals *MS Thesis* University of Maryland, College Park

[8] Barrett R M 1990 Intelligent rotor blade actuation through directionally attached piezoelectric crystals *AHS National Forum (Washington, DC) 1990*

[9] Barrett R M 1995 Method and apparatus for structural actuation and sensing in a desired direction *US Patent 5,440,193* initial filing February 1990, issued August 1995

[10] Chen P C and Chopra I 1993 A feasibility study to build a smart rotor: induced-strain actuation of airfoil twist using piezoceramic crystals *Proc. SPIE North American Conf. on Smart Structures and Materials (Albuquerque, NM) 1993* vol 1917, pp 238–54

[11] Park C, Walz C and Chopra I 1993 Bending and torsion models of beams with induced strain actuators *Proc. SPIE North American Conf. on Smart Structures and Materials (Albuquerque, NM) 1993* vol 1917, pp 192–216

[12] Chen P C and Chopra I 1994 Induced strain actuation of composite beams and rotor blades with embedded piezoceramic elements *Proc. SPIE North American Conf. on Smart Structures and Materials (Orlando, FL) 1994* vol 2190, pp 123–40

[13] Chen P C and Chopra I 1995 Hover testing of a smart rotor with induced-strain actuation of blade twist *Proc. 36th AIAA/ASME/ASCE/AHS/ASC Structures, Structural Dynamics and Materials Conf. and AIAA/ASME Adaptive Structures Forum, AIAA-95-1097 (New Orleans, LA) 1995*

[14] Spangler R L and Hall S R 1990 Piezoelectric actuators for helicopter rotor control*Paper Proc. 31st AIAA/ASME/ASCE/AHS/ASC Structures, Structural Dynamics and Materials Conf. (Long Beach, CA) 1990*

[15] Barrett R 19– Active plate and missile wing research using EDAP elements *Smart Mater. Struct.* **1** 214–26

[16] Barrett R 1994 Active plate and missile wing development using DAP elements *AIAA J.* **32** 601–9

[17] Barrett R 1993 Aeroservoelastic DAP missile fin development *Smart Mater. Struct.* **2** 55–65

[18] Barrett R 1993 Modeling techniques and design principles of a low aspect ratio active aeroservoelastic wing *Proc. SPIE North American Conf. on Smart Materials and Structures (Albuquerque, NM) 1993* vol 1917, pp 107–18

[19] Barrett R 1993 Active composite torque-plate fins for subsonic missiles *Dynamic Response of Composite Structures Conf. (New Orleans, Louisiana) 1993*

[20] Barrett R 1993 Advanced low-cost smart missile fin technology evaluation *Final Report to Wright Laboratory* USAF Armament Directorate, contract number F08630-93-C-0039 Eglin AFB FL

[21] Barrett R 1994 All-moving active aerodynamic surface research *Proc. 31st Annual Technical Meeting of the Society of Engineering Science (College Station, TX) 1994* pp 2–15

[22] Barrett R 1994 A solid state apparatus for controlling pitch deflections of aerodynamic flight control surfaces *Auburn University Invention Disclosure* patent pending

[23] Barrett R, Gross R S and Brozoski F 1996 Missile flight control using active Flexspar actuators *Smart Mater. Struct.* **5** 121–28

[24] Barrett R, Gross R S and Brozoski F T 1995 Design and testing of subsonic all-moving smart flight control surfaces *Proc. 36th AIAA Structures, Structural Dynamics and Control Conf. (New Orleans, LA) 1995* pp 2289–96

[25] Jones R M 1975 Micromechanical behavior of a lamina *Mechanics of Composite Materials* (New York: Hemisphere)